Rapid Communications

Phase diagram topology of the Haldane-Hubbard-Coulomb model

Igor S. Tupitsyn and Nikolay V. Prokof'ev
Department of Physics, University of Massachusetts, Amherst, Massachusetts 01003, USA
and Russian Research Center "Kurchatov Institute," 123182 Moscow, Russia

(Received 4 September 2018; revised manuscript received 18 March 2019; published 28 March 2019)

We study the phase diagram of the interacting spin-1/2 Haldane model with chiral phase $\phi = \pi/2$ at half-filling. Both on-site and long-range Coulomb repulsive interactions (Haldane-Hubbard-Coulomb model) are considered. The problem with on-site interaction U alone was addressed in the past by a variety of approximate and finite-size methods that produced results in disagreement with each other both quantitatively and qualitatively. Here we employ the diagrammatic Monte Carlo technique to accurately locate phase transition points to the topologically nontrivial phases in the (Δ, U) plane, where $\pm\Delta$ is the inversion symmetry breaking on-site energy, and establish that momentum dependence of self-energy cannot be neglected in the proper treatment. We also find that even modest long-range interactions, typically discarded in theoretical considerations, result in significant shifts of transition lines.

DOI: 10.1103/PhysRevB.99.121113

Introduction. The Haldane model [1] was invented to introduce the integer quantum Hall effect without Landau levels. It describes noninteracting spinless electrons on the honeycomb lattice with nearest-neighbor (NN) and next-nearest-neighbor (NNN) hopping amplitudes and inversion symmetry breaking on-site energy terms $\pm\Delta$ [see Fig. 1(a)]. The NN amplitude t_1 is real and the NNN amplitude $t_2 e^{\pm i\phi}$ is complex, with chiral phase ϕ. Complex $t_2 e^{\pm i\phi}$ opens a gap at the Dirac points (the same effect is achieved by nonzero Δ) and breaks the time-reversal symmetry. The resulting model features topologically trivial and nontrivial phases in the (Δ, ϕ) plane, and constitutes the simplest example of a Chern insulator [2].

Its natural generalization to interacting spin-1/2 fermions, the Haldane-Hubbard model (see, for instance, Ref. [3]), is considered as one of the key models for studying topological phases and transitions between them in condensed-matter physics. In recent years it has been intensively studied by various analytical and numerical methods that were either approximate, such as mean-field (MF) and dynamic mean-field theories (DMFT), or capable of solving only relatively small system sizes (exact diagonalization) (see Ref. [4]). Unfortunately, these calculations produce results that radically disagree with each other quantitatively, and sometimes even lead to qualitative discrepancies. For conventional quantum Monte Carlo methods simulating finite-size systems, the complex hopping amplitude t_2 renders them inefficient due to the notorious fermionic sign problem.

In general, similarly to the case of the ionic Hubbard model [5] where $t_2 = 0$, we expect topologically trivial band and Mott insulator phases in the limit of large Δ and U, respectively (here U is the strength of on-site repulsion). In between the two limiting cases, a variety of topologically nontrivial and exotic intermediate states were proposed [see, for instance, Refs. [3,6–8]]. However, some of these states appear to be "method specific"; a notable exception is a topologically nontrivial phase with spontaneously broken spin-rotation $SU(2)$ symmetry that is found in most mean-field studies [3,7,9]. The problem of identifying possible intermediate phases of the Haldane-Hubbard model in the selected region of parameters, including the one with spontaneously broken spin-rotational symmetry, has been recently addressed in Ref. [4] by three alternative methods: MF, exact diagonalization (ED), and single-site DMFT. While all three methods agreed on the identification of possible intermediate phases, they otherwise demonstrated radical quantitative differences in positions of the corresponding critical points and lines (see Fig. 2 in [4]).

In this Rapid Communication we employ the bold diagrammatic Monte Carlo technique (BDMC) developed for graphene-type systems [10] to (i) study the phase diagram of the Haldane-Hubbard model for the same values of hopping amplitudes as in Ref. [4] and (ii) demonstrate the effect of the often neglected Coulomb interaction (the corresponding Hamiltonian can be referred to as the Haldane-Hubbard-Coulomb model). The BDMC technique is not subject to the conventional fermionic sign problem [11,12] and allows one to deal with interaction potential of arbitrary shape in an approximation-free manner [13]. The accuracy of final results is controlled by convergence of results with increasing the expansion order. This approach does work in the most interesting part of the phase diagram away from the Mott insulating phase.

Model. The spin-1/2 Haldane model on the honeycomb lattice is based on the tight-binding approximation:

$$\begin{aligned} H_0 = &-t_1 \sum_{\langle \mathbf{ij}\rangle\sigma} (a^\dagger_{\mathbf{i}\sigma} b_{\mathbf{j}\sigma} + \text{H.c.}) \\ &- t_2 \sum_{\langle\langle \mathbf{ij}\rangle\rangle\sigma} e^{i\eta_{ij}\phi} (a^\dagger_{\mathbf{i}\sigma} a_{\mathbf{j}\sigma} + b^\dagger_{\mathbf{i},\sigma} b_{\mathbf{j},\sigma} + \text{H.c.}) \\ &+ \Delta \sum_{\mathbf{i},\sigma} \xi(i)\, n_{\mathbf{i}\sigma} - \sum_{\mathbf{i}\sigma} \mu_\sigma n_{\mathbf{i}\sigma}. \end{aligned} \tag{1}$$

The geometry, lattice vectors, and sublattice $A-B$ notations are explained in Fig. 1(a). Here $\xi(i \in A) = +1$, $\xi(i \in$

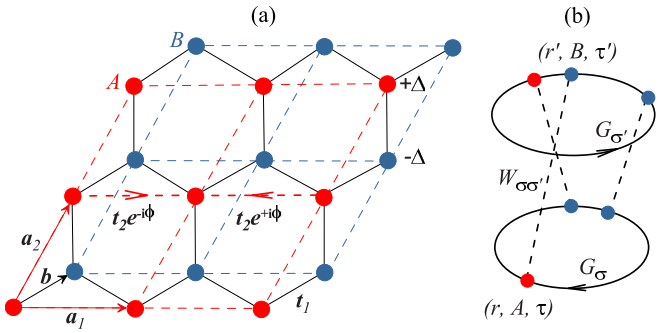

FIG. 1. (a) Decomposition of the honeycomb lattice into two shifted triangular sublattices A and B. Lattice spacing $|\mathbf{a}_1| = |\mathbf{a}_2| = a$ is used as a unit of length. The NN hopping, t_1, is real, and the NNN hopping $t_2 e^{\pm i\phi}$, is complex, with phase $+\phi$ corresponding to counterclockwise winding within the hexagon. The staggered on-site energy $\pm\Delta$ has opposite sign on sublattices A and B. (b) Typical third-order skeleton diagram for free energy with $\mathbf{r}$ and τ standing for the unit-cell index and imaginary time, respectively.

$B) = -1$, and μ_σ is the chemical potential for spin component $\sigma = \uparrow, \downarrow$. The sign of the phase of the NNN hopping amplitude, $\eta_{ij} = \pm$, depends on the winding direction [see Fig. 1(a)]. We employ standard second-quantization notations for creation, annihilation, and density operators in the site representation for sublattices A and B.

In what follows we consider an interacting problem, $H = H_0 + H_{\rm int}$, with

$$H_{\rm int} = \frac{1}{2}\sum_{\mathbf{ij}\sigma\sigma'} V_{\sigma\sigma'}(|\mathbf{r_i} - \mathbf{r_j}|) n_{\mathbf{i}\sigma} n_{\mathbf{j}\sigma'}. \qquad (2)$$

The on-site Hubbard repulsion term $V_{\sigma\sigma'}(0) = U\delta_{\sigma,-\sigma'}$ explicitly depends on spin indices, while $V_{\sigma\sigma'}(|\mathbf{r_i} - \mathbf{r_j}| > 0) = U_C|\mathbf{b}|/|\mathbf{r_i} - \mathbf{r_j}|$ [see Fig. 1(a)] describes the spin-independent Coulomb tail. Depending on the value of U_C, zerovs nonzero, Eqs. (1) and (2) describe the spin-1/2 Haldane-Hubbard or Haldane-Hubbard-Coulomb models.

Formalism. The BDMC technique employed here is based on stochastic sampling of skeleton diagrams based on fully dressed Green's functions, G, and screened interactions, W, or the so-called G^2W skeleton expansion [14] [see Fig. 1(b)]. At any order of expansion, N, self-consistency is reached by solving Dyson equations that take an algebraic form in the Matsubara frequency-momentum space:

$$G^{-1} = G_0^{-1} - \Sigma\,, \quad W^{-1} = V^{-1} - \Pi, \qquad (3)$$

where Σ is the self-energy and Π is the polarization function (both are matrices in the spin and sublattice space). Final results with controlled accuracy are obtained by computing vertex corrections from higher-order diagrams until convergence is reached. We omit here further technical details as they are fully documented in Refs. [13,15], and, in application to graphene systems, in Ref. [10]. The BDMC technique used in this work was carefully benchmarked against hybrid Monte Carlo results for graphene-type systems [16] (see Fig. 2 in Ref. [10]), and we established that even in the most difficult parameter regime near the semimetal-insulator transition our data were converging to known answers at the level of the third skeleton order.

To obtain the phase diagram in the (Δ, U) plane we compute the Chern numbers C^σ and renormalized electronic dispersions for both spin projections; transitions between topologically trivial and nontrivial phases manifest themselves by both changing the integer value of C^σ and by closing the bulk gap at Dirac points. These quantities can be computed by knowing the fully dressed Green's functions that are the direct outcome of the BDMC simulations. Following Refs. [17,18], Chern numbers for an interacting system can be extracted from properties of the so-called topological Hamiltonian, $\mathcal{H}_T = -G(i\omega \to 0, \mathbf{k})^{-1}$, assuming that transitions in question are of the "band-structure" type. The zero-frequency limit is obtained by extrapolating finite-temperature data for the set of smallest fermionic Matsubara frequencies, $\omega_n = 2\pi T(n + 1/2)$, with integer n and temperature T (see Fig. 1 in the Supplemental Material [19]). Eigenstates of $\mathcal{H}_T$ then allow one to compute C^σ by using the gauge-invariant method developed in Ref. [20].

In the Haldane model C^σ can take values 0 and 1. In what follows we consider the total Chern number, $\mathcal{C} = C^\uparrow + C^\downarrow$, as a topological order parameter whose allowed values 0, 1, and 2 distinguish phases. Our calculations are performed at half-filling for system sizes $L^2 = 16^2$ and 32^2 (the number of sites is $2L^2$) with periodic boundary conditions and at temperatures $T/t_1 = 0.1$ and 0.05, to quantify finite-size and finite-temperature effects. Chern numbers calculated for our system parameters using the method of Ref. [20] are integers with accuracy better than 10^{-8}. We take $t_1 = 1$ as the unit of energy and fix $t_2 = 0.2$ and $\phi = \pi/2$, as in Ref. [4]. We had to limit our analysis to on-site repulsion $U < 7$; obtaining converged answers at larger values of U requires reformulation of the diagrammatic expansion and goes beyond the scope of present work.

Haldane-Hubbard model. We first study the phase diagram of the Haldane-Hubbard model (1)-(2) when $U_c = 0$, and concentrate on the topologically nontrivial intermediate Chern insulator states away from the Mott insulator. To obtain transition lines separating the band and Chern insulators we fix U and find where the total Chern number changes its integer value along the Δ axis. If we only account for the first-order diagrams, equivalent to the so-called fully self-consistent GW approximation, then we do not see the topologically nontrivial phase $\mathcal{C} = 1$ with spontaneously broken spin-rotational symmetry. Next-order vertex corrections do not change this outcome either; i.e., at the level of two lowest orders the skeleton diagram results are consistent with the DMFT calculations, but plainly contradict the MF and ED predictions [4]. This is a clear sign that precise location of the point where all three phases meet cannot be determined reliably by approximate methods.

To locate the $\mathcal{C} = 1$ phase and eliminate the first-order transition scenarios we employ the following strategy. In one set of simulations we break the spin-rotational symmetry explicitly by making the hopping amplitudes spin dependent:

$$t_{1,2}(\uparrow) \to t_{1,2}(\uparrow)/\delta^{1/2}, \quad t_{1,2}(\downarrow) \to t_{1,2}(\downarrow)\delta^{1/2}, \quad \text{with } \delta > 1.$$

In this case, the $\mathcal{C} = 1$ phase exists even at $U = 0$, but for $U > 4$ converged answers are obtained only by accounting for

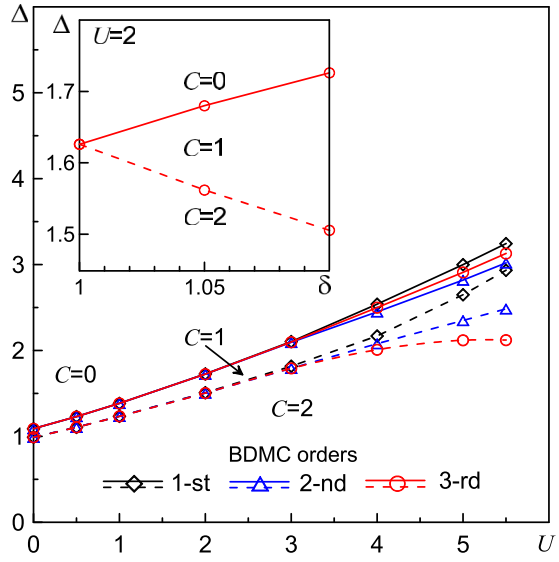

FIG. 2. Chern insulator phases ($\mathcal{C} = 2, 1$) of the Haldane-Hubbard model with explicitly broken spin-rotational symmetry ($\delta = 1.1$; see text) in different skeleton orders ($\mathcal{C} = 0$ corresponds to the topologically trivial band insulator phase). In the inset we show how the size of the $\mathcal{C} = 1$ phase for $U = 2$ shrinks with the value of spin-imbalance parameter δ. Statistical and systematic errors in this and other figures are smaller than symbol sizes.

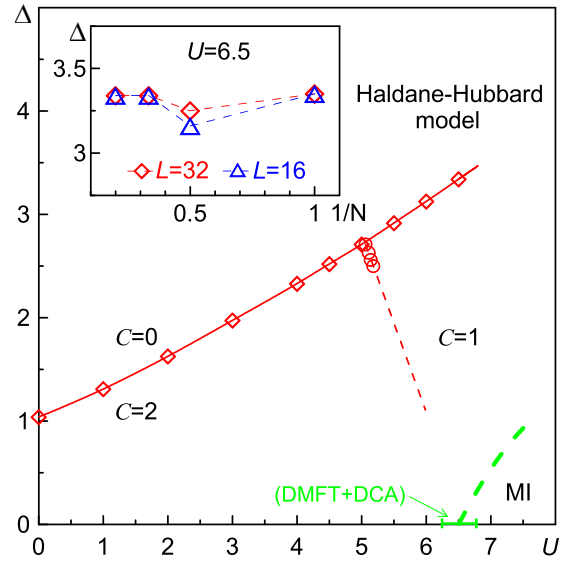

FIG. 3. Phase diagram of the $SU(2)$-symmetric Haldane-Hubbard model. Solid red line with diamonds separates the topologically trivial band ($\mathcal{C} = 0$) from Chern insulator phases. Dashed red line with circles separates Chern insulators with preserved ($\mathcal{C} = 2$) and spontaneously broken ($\mathcal{C} = 1$) spin-rotational symmetries. Dashed line is extrapolated toward the first-order transition between the $\mathcal{C} = 1$ and Mott insulator phases shown by the green dashed line, as established in Refs. [4,22] by the DMFT (for $\Delta \neq 0$) and dynamic cluster approximation (for $\Delta = 0$) methods. In the inset we show how the position of the critical line at $U = 6.5$ depends on the inverse skeleton expansion order $1/N$. Within the chosen accuracy of 0.1 we see no difference in converged answers for linear system sizes $L = 32$ and 16 (as well as for temperatures $T = 0.1$ and 0.05).

high-order diagrams (up to fifth order), since the behavior at $N = 2$ and $N = 3$ is different (see Fig. 2). We then use the solutions for G, Σ, and Π to initialize calculations with smaller spin imbalance all the way to $\delta = 1$ (no spin imbalance) to see if the $\mathcal{C} = 1$ phase survives. We follow this protocol for all values of $U \leqslant 5.5$. In the second set of simulations we start with $\delta = 1$ and monitor how results change with increasing N, in particular, how the $\mathcal{C} = 1$ state appears in some region of parameters and remains stable. The second protocol is applied at $U \geqslant 4$.

Following the first protocol, we determine that the $\mathcal{C} = 1$ phase goes away as $\delta \to 1$ for all values of $U < 5$; see a typical data set for $U = 2$ in the inset of Fig. 2. This rules out the phase diagram topology predicted by the ED studies of small clusters [4] (apparently, the momentum space resolution was too sparse to conclusively eliminate the $\mathcal{C} = 1$ state in this parameter regime). In the second ($\delta = 1$) protocol, the $\mathcal{C} = 1$ phase opens up only in simulations performed at $U > 5$ with $N \geqslant 3$.

Results obtained within both protocols are summarized in Fig. 3. The transition line, separating the band and Chern insulators, is rather close to the one obtained in Ref. [4] within the single-site DMFT. The $\mathcal{C} = 1$ phase does exist, but the critical on-site repulsion, U_m, where this phase first emerges and the two transition lines meet is found to be close to $U_m \approx 5$. This value is nearly three times smaller than the single-site DMFT result for U_m, indicating that momentum dependence of self-energy plays an important role in the quantitative analysis. The MF prediction $U_m \sim 4$ happens to be closer to the correct answer, but the slope of the ($\mathcal{C} = 2$)-($\mathcal{C} = 1$) line has an opposite sign.

If we extrapolate the upper part of the transition line between the $\mathcal{C} = 2$ and $\mathcal{C} = 1$ phases toward larger values of U, we hit the first-order transition to the Mott insulator state as determined in Refs. [21,22], in overall agreement with the ED picture. Unfortunately, the G^2W skeleton expansion implemented here does not work in the vicinity of the Mott state, and we can only rely on extrapolation from a limited set of data. The breakdown of the self-consistent expansion at $\Delta < 2$ and $U > 5.5$ is established by detecting that the series generated at the largest simulation order reach its convergence radius (see Ref. [23]). For the upper part of the phase diagram the skeleton expansion converges exponentially fast (see the inset in Fig. 3). We attribute this behavior to the band-structure-type origin of the topological transitions in the corresponding parameter range, which also justifies the protocol of evaluating the Chern number within the effective Hamiltonian approach [17,18,20]. (Typical behavior of the proper self-energy as a function of frequency in the vicinity of the Dirac point momentum is shown in Fig. 1 of the Supplemental Material [19]; when extrapolated to zero frequency it produces a Hermitian matrix in the spin and sublattice spaces.)

Haldane-Hubbard-Coulomb model. We now proceed with the study of long-range interaction effects and consider nonzero values of U_C in (2). To ensure that the repulsive potential is monotonously decreasing with distance we take $U_C \leqslant U$ (by definition, U_C is the strength of the NN interaction). The most obvious effect of the Coulomb potential

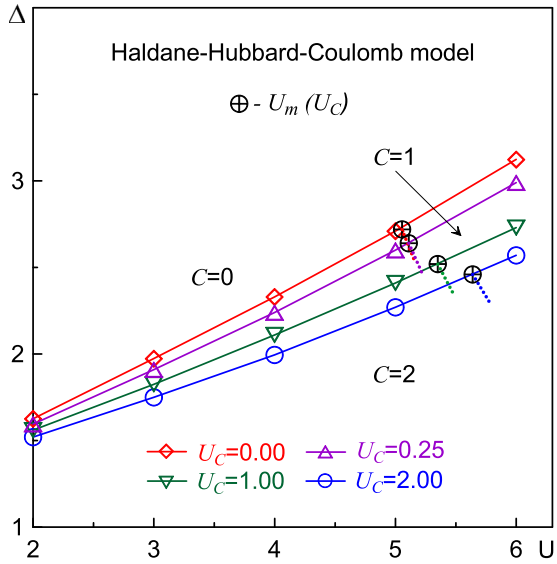

FIG. 4. Effect of the long-range Coulomb potential, $V_{\sigma\sigma'}(r > 0)$, on the phase diagram. Solid lines with symbols separate the topologically trivial band and nontrivial Chern insulators for different values of the Coulomb coupling U_C. Black circles with crosses mark positions of critical points $U_m(U_C)$, separating the Chern phases with $\mathcal{C} = 2$ and $\mathcal{C} = 1$. Dotted lines show upper parts of the transition lines between the $\mathcal{C} = 2$ and $\mathcal{C} = 1$ phases for corresponding values of U_C.

can be understood as follows. Imagine that we add a constant interaction term V_C at all distances $|\mathbf{r}_i - \mathbf{r}_j| > 0$ (i.e., an infinite-range potential) to the Haldane-Hubbard model. This would be equivalent to simply shifting the chemical potential of the model by V_C and reducing the value of the on-site repulsion to $U - V_C$. Correspondingly, under this transformation the entire solid line is translated horizontally, $\Delta(U, V_C) = \Delta(U - V_C, 0)$, and thus appears shifted downward in the (Δ, U) plane, as in Fig. 4. However, this thinking is only valid qualitatively; the horizontal-shift transformation strongly overestimates the downward shift and fails to explain the correct locations of special points $U_m(U_C)$ (squares with crosses do not form a horizontal line).

Overall, Coulomb interactions suppress the $\mathcal{C} = 1$ phase and push it to higher values of U and lower values of Δ. Given that in realistic materials the ratio between the U and U_C parameters is not small, Coulomb effects cannot be neglected or easily (as in the above example with constant shift at $r > 0$) accounted for in quantitatively accurate predictions.

Conclusions. We investigated the phase diagram of the spin-1/2 Haldane model on honeycomb lattice with on-site and long-range Coulomb interactions by the bold diagrammatic Monte Carlo method to obtain results with controlled accuracy for convergent skeleton sequences. We confirmed the existence of topologically nontrivial intermediate phase with spontaneously broken spin-rotation $SU(2)$ symmetry, where the Chern numbers for two spin components are 0 and 1, resulting in the total Chern number $\mathcal{C} = 1$. This phase emerges only after we account for vertex corrections beyond the second G^2W skeleton expansion, indicating that any approximate theoretical scheme would be prone to large quantitative errors. Indeed, for the Haldane-Hubbard model we found that the transition between the band insulator, $\mathcal{C} = 0$, and $\mathcal{C} = 1$ phases takes place at $U = U_m \sim 5$, nearly a factor 3 smaller than the U_m value predicted by the single-site dynamic mean-field theory [4], which neglects the momentum dependence of the self-energy. The coarse-grained structure of the obtained phase diagram is close to that revealed by exact diagonalization [4] except for artifacts of momentum quantization in small clusters that prevent one from observing a direct $\mathcal{C} = 0 \longleftrightarrow \mathcal{C} = 2$ transition.

In the case of the Haldane-Hubbard-Coulomb model we quantified effects of typically neglected long-range Coulomb interactions. Both topologically nontrivial phases survive, but the $1/r$ potential tends to suppress topological phases in favor of the band insulator one and shifts the $\mathcal{C} = 1$ phase toward larger values of on-site repulsion. While remaining quantitative, Coulomb effects cannot be neglected if one aims at accurate predicting for real materials.

This is the first application of the BDMC technique to properties of interacting topological insulators. Given that it is applicable to both doped and undoped systems with arbitrary dispersion relation and shape of interaction potential, in future work it would be interesting to study the Haldane-Hubbard-Coulomb model at other filling factors and values of ϕ, and explore cases with "flat band" dispersion relevant to the search for fractional Chern insulator states (fractional quantum Hall effect without Landau levels) [24]. Our technique is directly applicable to these type of problems [15].

Acknowledgments. We thank T. Sedrakyan for discussions. This work was supported by the Simons Collaboration on the Many Electron Problem, the National Science Foundation under Grant No. PHY-1314735, and the MURI Program "New Quantum Phases of Matter" from AFOSR.

[1] F. D. M. Haldane, Phys. Rev. Lett. **61**, 2015 (1988).
[2] T. Thonhauser and D. Vanderbilt, Phys. Rev. B **74**, 235111 (2006).
[3] J. He, Y.-H. Zong, S.-P. Kou, Y. Liang, and S. Feng, Phys. Rev. B **84**, 035127 (2011).
[4] T. I. Vanhala, T. Siro, L. Liang, M. Troyer, A. Harju, and P. Törmä, Phys. Rev. Lett. **116**, 225305 (2016).
[5] S. S. Kancharla and E. Dagotto, Phys. Rev. Lett. **98**, 016402 (2007).
[6] J. He, S.-P. Kou, Y. Liang, and S. Feng, Phys. Rev. B **83**, 205116 (2011).
[7] J. He, Y. Liang, and S.-P. Kou, Phys. Rev. B **85**, 205107 (2012).
[8] C. Hickey, L. Cincio, Z. Papić, and A. Paramekanti, Phys. Rev. Lett. **116**, 137202 (2016).
[9] D. Prychynenko and S. Huber, Physica B **481**, 53 (2016).
[10] I. S. Tupitsyn and N. V. Prokof'ev, Phys. Rev. Lett. **118**, 026403 (2017).
[11] N. Prokofev and B. Svistunov, Phys. Rev. Lett. **99**, 250201 (2007).

[12] R. Rossi, N. Prokof'ev, B. Svistunov, K. Van Houcke, and F. Werner, Europhys. Lett. **118**, 10004 (2017).
[13] I. S. Tupitsyn, A. S. Mishchenko, N. Nagaosa, and N. Prokof'ev, Phys. Rev. B **94**, 155145 (2016).
[14] L. Hedin, Phys. Rev. **139**, A796 (1965).
[15] S. A. Kulagin, N. Prokof'ev, O. A. Starykh, B. V. Svistunov, and C. N. Varney, Phys. Rev. Lett. **110**, 070601 (2013); Phys. Rev. B **87**, 024407 (2013).
[16] M. V. Ulybyshev, P. V. Buividovich, M. I. Katsnelson, and M. I. Polikarpov, Phys. Rev. Lett. **111**, 056801 (2013).
[17] Z. Wang and S.-C. Zhang, Phys. Rev. X **2**, 031008 (2012).
[18] Z. Wang and B. Yan, J. Phys.: Condens. Matter **25**, 155601 (2013).
[19] See Supplemental Material at http://link.aps.org/supplemental/10.1103/PhysRevB.99.121113 for the proper self-energy as a function of frequency.
[20] T. Fukui, Y. Hatsugai, and H. Suzuki, J. Phys. Soc. Jpn. **74**, 1674 (2005).
[21] C. N. Varney, K. Sun, M. Rigol, and V. Galitski, Phys. Rev. B **82**, 115125 (2010).
[22] J. Imriska, L. Wang, and M. Troyer, Phys. Rev. B **94**, 035109 (2016).
[23] R. Rossi, F. Werner, N. Prokof'ev, and B. Svistunov, Phys. Rev. B **93**, 161102(R) (2016).
[24] E. J. Bergholtz and Z. Liu, Int. J. Mod. Phys. B **27**, 1330017 (2013).